Nanoscale

FEATURE ARTICLE

View Article Online
View Journal

Cite this: DOI: 10.1039/c4nr02419b

Impact of optical antennas on active optoelectronic devices

Alireza Bonakdar and Hooman Mohseni*

Remarkable progress has been made in the fabrication and characterization of optical antennas that are integrated with optoelectronic devices. Herein, we describe the fundamental reasons for and experimental evidence of the dramatic improvements that can be achieved by enhancing the light-matter interaction *via* an optical antenna in both photon-emitting and -detecting devices. In addition, integration of optical antennas with optoelectronic devices can lead to the realization of highly compact multifunctional platforms for future integrated photonics, such as low-cost lab-on-chip systems. In this review paper, we further focus on the effect of optical antennas on the detectivity of infrared photodetectors. One particular finding is that the antenna can have a dual effect on the specific detectivity, while it can elevate light absorption efficiency of sub-wavelength detectors, it can potentially increase the noise of the detectors due to the enhanced spontaneous emission rate. In particular, we predict that the detectivity of interband photon detectors can be negatively affected by the presence of optical antennas across a wide wavelength region covering visible to long wavelength infrared bands. In contrast, the detectivity of intersubband detectors could be generally improved with a properly designed optical antenna.

Received 9th May 2014
Accepted 11th July 2014

DOI: 10.1039/c4nr02419b

www.rsc.org/nanoscale

1. Introduction

The past decade has witnessed a rapid growth in the field of optical antennas, as they have proven to be excellent tools for manipulating the propagation of light and its interaction with electrons in matter. The inherent abilities of optical antennas, combined with rapid advances in nanotechnology, have led to its widespread application in many (bio-)molecular sensing,[1,2] photonics[3,4] and optoelectronic devices.[5,6] At a more fundamental level, these devices can be divided into passive and active categories. Passive devices are inherently linear (*e.g.* flat optics[7] and transformational optics[8]), while active devices are non-linear and incoherent (*e.g.* photodetectors[9,10]). Here, we focus on the application of optical antennas in active optoelectronic devices. The non-linear nature of active devices is

Northwestern University, 2145 Sheridan Rd, Evanston, Illinois, USA. E-mail: hmohseni@northwestern.edu

Alireza Bonakdar is a PhD candidate currently working in the Bio-inspired Sensors and Optoelectronics Laboratory (BiSOL) at Northwestern University under the supervision of Professor Hooman Mohsen. His research is to design and develop novel optical antennas, which can enhance the quantum efficiency of an ultra-small quantum infrared photodetector. In addition, his research interest involves the design and development of a new class of optical antenna—the optomechanical nanoantenna, which leads to ultra-fast and highly compact optical nanoswitches.

Hooman Mohseni is a professor of Electrical Engineering and Computer Sciences at Northwestern University. He is the recipient of several research and teaching awards, including NSF CAREER Award, DARPA Young Faculty Award, and Northwestern Faculty Honor Roll. Mohseni serves at the editorial boards of IEEE Photonics, IEEE Selected Topics in Quantum Electronics, Optics Letter, and Frontiers in Material. He has published over 115 peer-reviewed articles in major journals, including Nature, Nano Letters, and ACS Nano. He holds 14 issued US and International patents. He is a fellow of SPIE and OSA.

responsible for their ability to amplify or transducer the optical signal, as well as to convert optical power to electrical power, or *vice versa*.

As we will see in the following sections, many interesting active optical devices have two major dimensional requirements: a large (microscale) optical component and a small (nanoscale) quantum absorber/emitter. The former is needed for efficient coupling of light to/from a distance, and the latter can significantly improve the sensitivity of the device. The dimension contrast is inherently related to the difference in photonic and electronic wave-functions, and in the absence of a coupler, it results in a weak coupling between the two. The inefficient light-matter interaction can be enhanced using an optical antenna. Optical antennas can couple diffraction-limited far-field modes to sub-wavelength near-field modes in the vicinity of the nanoscale optical absorber/emitter. The sub-wavelength nature of the field near the antenna demands tight alignment, and hence, there is a preference for direct integration of the antenna to the device.

The brief history and the recent progress in integrating the optical antenna with the active optical device are the main motivations and subjects of this review article. In section 2, theoretical background is presented to explain the optical enhancement mechanism in the interaction between the far-field mode and the semiconductor nano-absorber/emitter. In section 3, we review two major categories of active devices with integrated optical antenna: light emitting and absorbing devices. However, the fundamental concept described in section 2 has been utilized in many other active devices, including modulators and switches.[11]

2. Optical antenna: background and the need for high efficiency and directivity

The weak interaction of light and matter is a double-edged sword. For example, it is responsible for our ability of chemical sensing and imaging across the universe; however, in contrast, it severely limits the sensitivity of our detectors, as we will see in section 3.3. It is, therefore, highly desirable to be able to increase this interaction strength selectively and where needed. Naturally, since most optical systems take advantage of the large propagation distance of light, a high directivity is desirable. Table 1 shows some of the key parameters of the emitter, medium, and absorber for the case of infrared imagers. Details will be provided in section 3.3.1, but note that the conventional receiver (*e.g.*, a piece of semiconductor) has a poor directivity compared to the incoming beam. Furthermore, the weak light-matter interaction leads to a rather large absorption length, which demands a large volume of semiconductor to ensure high quantum efficiency (QE). In the following section, we shall see that the weak interaction can be substantially enhanced with a proper optical antenna design *via* an enhanced local density of states (LDOS). Although many commonly used optical antenna designs (*e.g.* bowtie, bulls-eye, Yagi-Uda, *etc.*) can produce either a high QE or a high directivity, it is not easy to achieve both properties simultaneously. However, this is not a fundamental limitation, and we will show a design based on photonic jets[12] that can achieve both requirements simultaneously. This method should be useful in many other applications, such as molecular sensing and solar harvesting, since their parameters are quite similar to those listed in Table 1.

Table 1 Comparing optical properties of semiconductor integrated with different optical antenna

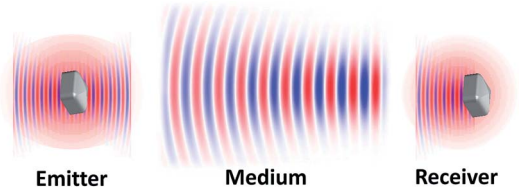

Properties	Emitter	Medium	Receiver
Material	Thermally excited atoms–molecules	Air	Semiconductor with bowtie with mettalo-dielectric
Light–matter interaction length L (μm)	$\sim 10^2$	$\sim 10^9$	~ 10 ~ 1 ~ 1
Relative LDOS	~ 10	~ 1	~ 10 $\sim 10^2$ $\sim 10^3$
Radiation directivity (dB)	~ 1.5	~ 20	~ 1.0 ~ 1.7 ~ 20

2.1. Near-field and far-field

An optical antenna is essentially a mode convertor that can efficiently couple free-space propagative modes to spatially confined near-field modes. Fig. 1 illustrates the schematic of the optical antenna functionality. A sub-wavelength quantum emitter/absorber is similar to its classical counterpart and the electrically small dipole and has a broad range of wave-vectors (due to the diffraction). This property leads to a spatial radiative beam with weak directionality. On the other hand, in many light trapping/extracting applications, the far-field optical mode is considered to be a propagative mode with high directionality consisting of a narrow range of wave-vectors. A highly directive antenna can establish efficient coupling between the widespread modes of the emitter/absorber and the desirable directional far-field. Due to the reciprocity principle, the antenna can operate both as a receiver of, or transmitter to, the far-field. The antenna–emitter/absorber interaction is significant at the near-field region of the antenna, where the antenna modes are dominant compared with the free-space propagative modes. Antenna modes can be propagative or evanescent waves, and they carry radiative and non-radiative power, as well as store electromagnetic (EM) energy. These properties are often characterized by the antenna quality factor and loss, as extensively discussed in the literature.[13] Antennas with large quality factor have low non-radiative and

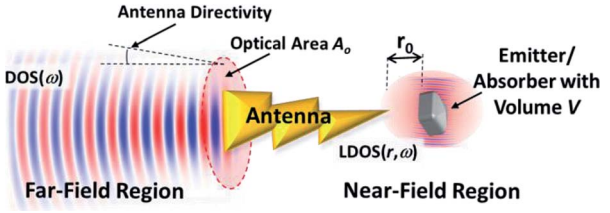

Fig. 1 Optical antennas couple far-field and the near-field and enhance extracting light from a quantum emitter or delivering it to a quantum load.

radiative antenna losses. At the first glance, the low radiative loss may seem to indicate a low coupling efficiency to the far-field. However, this is not true since the stored energy can be very large for antennas with large quality factor. In fact, a near unity coupling is possible, based on the coupled oscillator theory, but only at a very narrow spectral range. Since the minimum quality factor of the antenna is inversely proportional to its dimension (normalized to wavelength),[13] one can conclude that broadband antennas cannot be optically small.

We conclude that highly efficient and broadband antennas with high directivity, which are most desirable for the aforementioned application have to be optically large. All metallic antennas based on adiabatic mode conversion can satisfy the above performance at radio frequencies (*e.g.* horn antennas). However, large metal losses at the optical frequencies can significantly reduce the efficiency for an optically large, and all-metal optical antenna. This inherent limitations have recently motivated many research groups to develop metallo-dielectric hybrid antenna.[14,15]

2.2. Local density of states

In addition to the aforementioned mode coupling, an optical antenna can locally alter the photonic density of states (DOS). This property could be utilized to increase radiative power from/to a quantum emitter/absorber. In vacuum, DOS is a function of photon frequency, DOS $(\omega) = \omega_0^2/\pi^2c^3$, and it determines the number of available photonic states that an electronic dipole can spontaneously emit to. However, LDOS measures the geometrical and electromagnetic field effects on the locally available photon states by quantifying the electromagnetic energy density in the space and the polarization states. The value of LDOS for polarization state l can be defined as

$$\mathrm{LDOS}_l(\boldsymbol{r},\omega) = \sum_n \delta(\omega-\omega_n)\left(\varepsilon(\boldsymbol{r})\left|E_{n,l}(\boldsymbol{r})\right|^2 + \mu(\boldsymbol{r})\left|H_{n,l}(\boldsymbol{r})\right|^2\right) \quad (1)$$

where E_n and H_n are orthonormal eigenfields. ε and μ are electron permittivity and magnetic permeability, respectively. In the case of a cavity with a quality factor Q, $\delta(\omega-\omega_n)$ the function can be approximately replaced by a Lorentzian spectrum with $\Delta\omega = \omega/Q$.[16] The total DOS is the volume integration over space and summation over the polarization of LDOS, normalized to the volume of the space:[17]

$$\mathrm{DOS}(\omega) = \frac{1}{V}\sum_{l=1}^{3}\int \mathrm{LDOS}_l(\boldsymbol{r},\omega)d^3r \quad (2)$$

Importantly, the spontaneous emission rate of a dipole is proportional to LDOS,

$$\Gamma_{\mathrm{sp}} = \frac{\pi\omega_0}{3\varepsilon_0\hbar}\left|<a|\hat{\boldsymbol{\mu}}|b>\right|^2 \mathrm{LDOS}(\boldsymbol{r}_0,\omega_0) \quad (3)$$

where $\mu_{ba} = \left|<a|\hat{\boldsymbol{\mu}}|b>\right|$ is the dipole moment and $\hbar$ is the reduced Plank's constant.

Thus, the LDOS distribution in space determines the radiation enhancement/suppression due to the presence of polarizable objects, such as optical antenna. Fluctuation-dissipation theorem (FDT), which characterizes the small deviation of physical system from equilibrium point using equilibrium values, can also be used to calculate LDOS. Since LDOS is a property of the optical system that is quantified with equilibrium values, FDT-based approach gives the same results as in eqn (1). Fig. 2 shows LDOS as a function of distance from a sphere with a 100 nm diameter and made with three different materials.

Although LDOS is an important property of the microcavities, optical antennas and other photonic structures, a straightforward and universal definition of LDOS in a dissipative system has been subject to many debates and controversies for decades.[18–24] In practice, almost all materials in nature exhibit a certain level of optical loss. Specifically, in light trapping/extracting applications, such as photodetector and LED devices, considering the loss of the active region is crucial for a proper evaluation of LDOS. It should be emphasized that the definition of LDOS in eqn (1) is under the lossless condition, where eigenmodes are Hermitian and orthogonal,[17] allowing LDOS to be derived from the converging imaginary part of the system's Green's function.[25,26] However, in a lossy system, a set of orthogonal eigenmodes no longer exists to define LDOS as in eqn (1).[26] In addition, insertion of loss mixes both real and imaginary parts of Green's function, leading to the divergence of the imaginary part.[27] In general, there are two major approaches to resolve LDOS calculation issues in lossy systems.

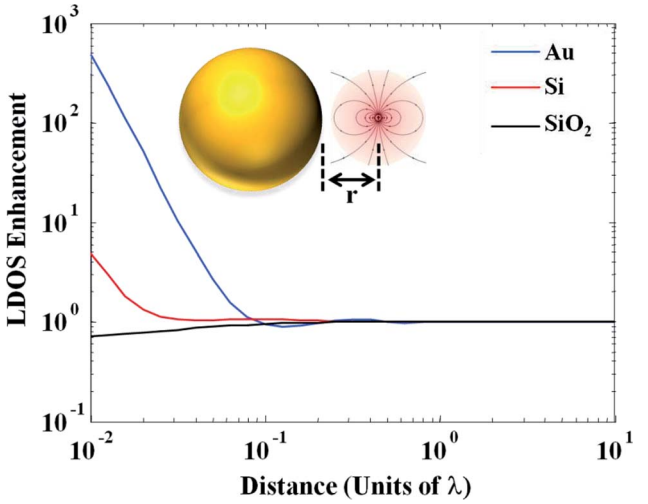

Fig. 2 LDOS as a function of distance from a 100 nm-diameter nanosphere for three different materials: metal (gold), semiconductor (Si) and insulator (SiO_2) and at a wavelength of $\lambda = 500$ nm.

The first approach is to circumvent the divergence issue of the imaginary part of Green's function, for example by introducing locally lossless homogeneous medium at the dipole position where LDOS is to be calculated.[14] The second approach is to redefine the LDOS formalism, for example by introducing a small set of quasi-normal modes[26] or replacing delta function by a finite line-width Lorentzian function.[17] In this paper, the latter approach is chosen to calculate LDOS at a dissipative medium. This approach is highly compatible with finite-difference-time-domain method.

In the same vein, circuit theory could be used to model and optimize optical antennas. Using this approach, it becomes evident that the impedance of the quantum emitter/absorber is quite different from the vacuum impedance. Antenna can adjust the impedance mismatch problem by behaving as an impedance matching circuit.[28,29]

2.3. Polarization sensitivity

Unlike semiconductors or microbolometers, optical antennas inherently incorporate polarization and angular momentum sensitivities. For many imaging applications, polarization sensitivity of photodetectors increases the contrast of targets *versus* background.[30] For example, polarization effect is an important physical property in the detection of small targets in a marine environment[31] as well as in cell biology.[32] Information contained in the polarization of a signal can be utilized for image segmentation, pattern recognition as well as 3D imaging.[33] However, for some applications where the level of a signal is very low, polarization sensitivity can drop the signal power below the detectable point. Therefore, antennas that can enhance light–matter interaction with insensitive polarization are sometimes desirable. Optical antennas with symmetry, such as the bull's eye antenna,[34] deep trench-thin metal array,[35] and nanohole array antenna[10] have insensitive or very small sensitivity to incoming polarization. In semiconductor lasers, where most photons have a well-defined polarization, optical antennas can be efficiently utilized. On the other hand, for LED and optical modulators, polarization sensitivity is considered as a limiting factor due to the random nature of the signal's polarization.

3. Integration of optical antenna with active devices

3.1. Semiconductor lasers with integrated optical antenna

Integrated optical antennas on laser sources have many advantages as they directly modify the near-field and far-field properties of the lasers' beams. Many applications could significantly benefit from such a modification, including microscopy, spectroscopy, nanoscale optical lithography, heat assisted magnetic recording, spatially resolved chemical imaging, and laser processing. The integration of optical antennas with lasers can be categorized into the far-field and the near-field modification of the lasers' output. Far-field modification of laser outputs is the goal of a large volume of researches, such as optical data recording, far-field optical microscopy, and laser beam shaping and collimation. On the other hand, near-field modification is mainly used for biological spectroscopy and molecular sensing as it provides great field enhancement at the near-field of an optical antenna. In the following section, we look at the major achievements in both areas.

3.1.1. Laser far-field modification. The initial motivation for the integration of the optical structure with a laser to modify its far-field goes back to the research efforts to reduce laser spot size in optical data recording technologies.[36,37] As an example, early work demonstrated the recording of 250 nm-diameter marks at 7.5 Gb per square inch by fabricating a very small aperture laser (VSAL) operating at $\lambda = 980$ nm with a 250 nm-square aperture at the facet of the laser.[36] VSAL was further investigated to realize a high-resolution far-field scanning optical microscope by controlling the focal length of the transmitted field's spot.[38,39] A main parameter in the evaluation of the quality of a laser beam at the far-field, in terms of divergence and directionality, is the directivity of the optical structure fabricated on the laser's facet. An aperture on the facet of a laser cannot enhance the directivity of the beam in the far-field, instead, it modifies the field's spatial distribution by the aperture's Fourier transformed shape. Directivity enhancement can be achieved by coherent interference between an array of optical elements and apertures, similar to a phased-array antenna in RF terminology.[40–43] For example, Guo *et al.* fabricated an optical antenna on a 650 nm wavelength commercial laser, which consists of a 300×500 nm^2 aperture and four concentric rings to focus the beam $\sim 2\lambda$ away from the laser's facet with a 140% intensity enhancement.[41] An edge-emitting semiconductor laser has an intrinsic beam divergence that limits the coupling efficiency of the beam to optical fibers and waveguides. Using an aperture–groove optical antenna on a quantum cascade laser (QCL) at 9.9 μm, Yu *et al.* reported ~25 times reduction in the beam spreading. The interference of the light radiated from the aperture with the light scattered by the 1D-grooves reduces the divergence angle to as little as 2.4 degrees in the direction of the grooves and increases the beam directivity by at least 10 dB.[43]

In order to collimate light cylindrically, concentric grooves have been implemented (Fig. 3a–b).[44] Additionally, the superposition of concentric rings results in multiple collimated beam generation in the far-field.[45,46] The same group has reported a similar optical antenna integrated on a high power QCL laser to collimate the far-field beam.[47] Since the orientation of the grooves determines the polarization of scattered light from individual grooves in the far-field, the polarization of the laser can be rotated relative to the groove orientation. For example, the combination of two sets of aperture grooves, tilted 45 degrees in opposite directions can produce a combination of linear and circular polarization[48] as shown in Fig. 3c and d. The concept of optical antenna integration on semiconductor lasers is also adapted to THz laser sources utilizing spoof plasmonics[49] and concentric circular grating.[50]

3.1.2. Laser near-field modification. Many applications, such as molecular sensing and low power switching can greatly benefit from a laser beam that is tightly confined within a sub-

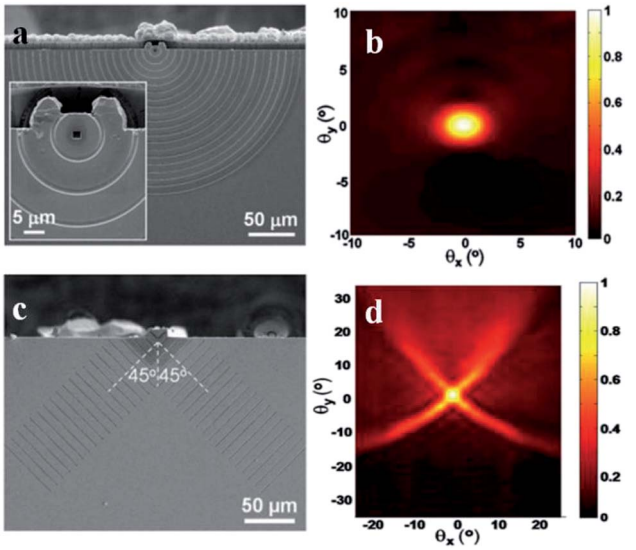

Fig. 3 Far-field modification using optical antenna integrated with quantum cascade lasers (QCL). (a and b) SEM image of concentric grooves with aperture on QCL and the measured far-field of the output laser. Reproduced with permission of the American Institute of Physics from ref. 38. (c and d) SEM image of two set of aperture grooves on QCL and the measured far-field that produces a combination of linear and circular polarization. Reproduced with permission of the American Institute of Physics from ref. 42.

wavelength volume. Very large confinements can be accomplished in the near-field, where evanescent modes exist. Although sub-wavelength apertures on facets of lasers can confine light, the coupling of the laser cavity modes to the near-field is very inefficient[51] since the optical transmission through a sub-wavelength aperture rapidly decays (it is proportional to the fourth power of the aperture size).[52] Unlike tiny apertures, optical antennas can efficiently convert laser power to the near-field and reduce the power loss. The first demonstration of optical antenna integration on an edge emitting laser was reported by Cubukcu *et al.*[51] where a coupled nanorod antenna was fabricated on the facet of a commercial near-infrared laser using focused ion beam (FIB) milling.

The application of such integrated optical antennas has been extended to biological imaging and spectroscopy by fabricating an integrated system in the mid-infrared region, where many biological and chemical molecules have absorption features.[53–58] This integration of optical antennas with active devices could propel lab-on-chip technology one step closer to fully integrated microsystems.[59] Recent progresses in QCLs have led to the realization of lasers with excellent properties in the mid- and long-infrared regions, where many important biomolecules have strong absorption features. However, the overall optical absorption of biomolecules is still very weak in their naturally occurring concentrations. Since mid and long-wave infrared detectors have poor sensitivity at room temperature, the aforementioned weak absorption cannot be detected with a system operating at room temperature. One of the ideas we developed to address this issue was to take advantage of the laser's non-linearity near its threshold and the strong coupling between the laser cavity mode and the optical antenna mode.

We initially fabricated and measured single[55] and coupled metal-oxide–metal antennas[54] on the facet of QCLs operating near λ of ~6 μm. Our experiments suggested that the perturbation of antenna's hot spot can affect the laser dynamic due to the strong coupling of the antenna and cavity modes. We then demonstrated a strong modulation of QCL cavity modes by perturbing the integrated optical antenna's near-field through an atomic force microscope (AFM) tip movement.[60] In this work, a non-linear feedback mechanism was shown to enhance the sensitivity in detecting molecules in the proximity of antenna. Fig. 4 shows a schematic of a bowtie antenna integrated on the facet of a QCL, and the relative position of the AFM tip. The AFM is operated on a non-contact mode with an amplitude oscillation of $\Delta d = 50$ nm near the antenna hot spot. As a result of AFM tip movement by about $\lambda/100$, laser power is modulated by ~74%, and its frequency shifts by $\Delta f \sim 30$ GHz. The figure of merit (FOM) of the frequency tuning of the laser in this experiment is $g = \Delta f/\Delta d \sim 6.4 \times 10^8$ Hz nm^{-1}, as shown in our time-resolved spectroscopy measurement (see Fig. 4). The measured FOM shows the extremely high modulation of laser operation caused by perturbing the antenna hot-spot due to the concentration of EM energy in the high LDOS in the antenna's near-field. The resultant FOM is about 10 times larger than the best results achieved by mechanically modifying the cavity modes.[61] More importantly, the volume of the moving part in our approach is about five orders of magnitude smaller.

Another interesting feature of an optical antenna is its ability to confine electromagnetic fields into a hot spot almost irrespective of their wavelengths. This property allows coinciding optical beams with very different wavelengths on non-linear media. Such a feature can be utilized for ultra-fast and low-power switching, wavelength mixing and converting by means of a non-linear element in the system. As an example, we

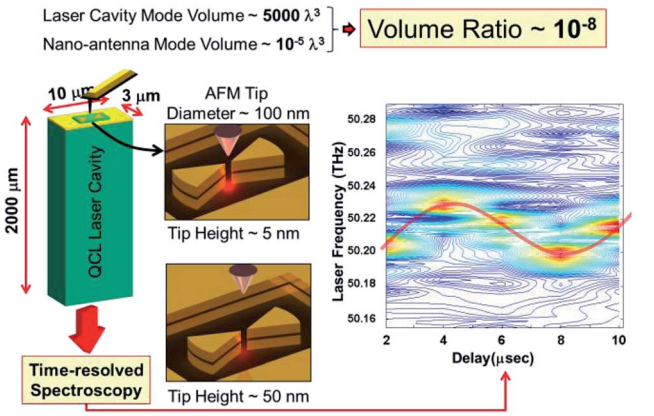

Fig. 4 Schematic of an integrated bowtie antenna with a QCL (left). Using time-resolved spectroscopy (right), we measured the frequency shift and intensity of QCL laser due to the mechanical motion of an atomic force microscope (AFM) tip (centre). Despite the extremely large volume difference between the antenna modes and laser cavity modes (about 10^{-8}), as well as the sub-wavelength motion of the AFM tip of ~$\lambda/120$, laser output is strongly modulated by the tip motion.

reported dynamic control of the near-field using a cross-polarized optical antenna integrated on a QCL laser.[62] The optical antenna is composed of two bowtie antennas resonating at 1.55 μm and 6 μm, as shown in Fig. 5a. A thin slab of germanium is fabricated at the antenna gap as the non-linear element. The near-field of a 6 μm wavelength QCL laser is controlled through free-carrier absorption induced in germanium by a 1.55 μm wavelength pumping light. The modulated, back-reflected signal from the laser is detected by an MCT detector before it is sent to a spectrum analyzer. Fig. 5e and f show the emitted power of the QCL laser at λ of ~6 μm modulated by a weak laser beam at 1.55 μm. The power dependency of the QCL emission to the polarization of the short wavelength beam clearly demonstrates the antenna's role.

3.2. Semiconductor LEDs with integrated optical antennas

One of the main limitations of light emitting diode (LED) is its low external quantum efficiency. This is partly due to the limited light extraction efficiency, which is the percentage of light that can leave the semiconductor and couple to the propagative optical modes. The second limiting factor is the small spontaneous radiation rate that allows other non-radiative mechanisms to consume a portion of the energy. Enhancing light extraction efficiency has been an intense field of research and different solutions have been developed. For example, using microlenses and by microstructuring the semiconductor, it has been enhanced by about one order of magnitude.[63] However, in order to reach the luminosity of fluorescent lamps or light bulbs, significant improvement is necessary for LEDs.[64] The motivation for the integration of optical antennas with LEDs is the desire to increase light emission from LEDs beyond the limited enhancement of conventional photonic methods. In early 1990, Kock *et al.* reported the first strongly directional emission from an infrared AlGaAs/GaAs surface-emitting LED *via* coupling to the surface plasmons.[65] They used a surface grating that acted like an antenna and provided efficient coupling of emitted photons from an electronic dipole to the far-field. It also enhanced the optical density of states, and subsequently, the spontaneous emission rate in the semiconductor.[66] In 2004, Okamoto *et al.* reported considerable light emission improvement from InGaN/GaN quantum wells, which were coated with plain and perforated thin films of silver.[64] Since then, a variety of antenna configurations are fabricated on the facets/surfaces of LEDs with different materials and emitting wavelengths.[67–69] The most challenging issue in using metallic antenna in this application is the large metal loss in the visible spectrum.[70]

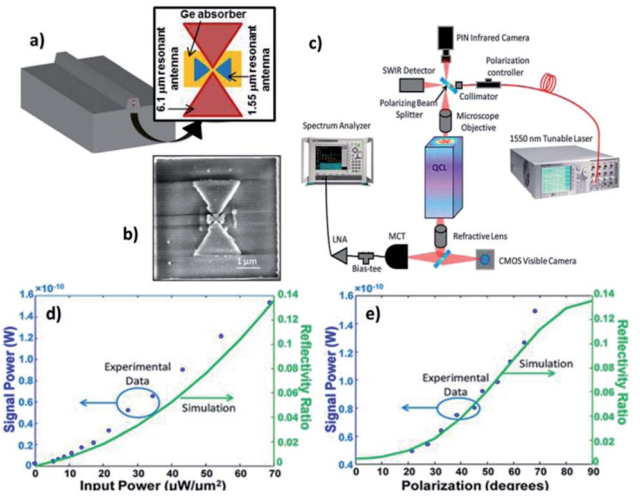

Fig. 5 (a) Schematic and (b) SEM image of a cross-polarized optical antenna operating at 1.55 μm and 6 μm integrated on QCL laser. (c) Schematic of the setup to measure the near-field and modulation field of the laser. (d) Modulation of back reflection 6 μm wavelength power from QCL laser as a function of 1.55 μm wavelength pumping power, (e) as a function of 1.55 μm wavelength polarization.

3.3. Semiconductor photodetectors with integrated optical antennas

Fast photodetectors with high sensitivity and QE are key elements in many modern applications, such as optical communication, optical interconnects, quantum key distribution and infrared imaging. Therefore, it is crucial to optimize the quantum efficiency-bandwidth product while maintaining low noise. Traditional photon detectors are optimized based on planar device geometry, where the optical (collection) area and the electrical (sensing) area are equal. Although increasing the material volume can increase the absorption and hence, the QE, the detector's overall performance is degraded by increases in power loss, latency, and noise.[9] In many conventional photodetectors, the device speed is limited by the carrier transit time, and a shorter transit time requires a thinner active region. Moreover, a thinner active region has smaller volume and hence a smaller dark current (noise). Unfortunately, a thinner active region means a smaller QE. A common approach to shrink the device size while maintaining a high QE is to use resonant cavities.[71,72] However, this approach can severely limit the optical bandwidth of the detector.

The main motivation in integrating optical antenna with photodetector is the need to surpass the aforementioned limitations and produce a very small (deep subwavelength) absorber with high QE, high directivity, high sensitivity (detectivity), and a broad optical bandwidth. As seen in section 2, optical absorption (QE) can be significantly enhanced in the presence of an optical antenna, due to the elevated LDOS. Unlike microcavities, this enhancement can be very broadband. Fortunately, optical antennas are quite efficient at longer wavelengths (due to the lower metal loss), and this is, in fact, the region that the semiconductor optical absorption is weaker.[73]

While the above idea has recently been studied by many groups, the effect of LDOS enhancement on the detector noise is commonly ignored. In section 2.2, we saw that LDOS enhancement leads to an increased radiative recombination rate, which leads to an increased generation rate due to the detailed balance principle. The increased carrier generation rate produces higher noise in the detector. This effect could be particularly significant for interband detectors, where the carrier lifetime is quite long.[74] In order to calculate the

sensitivity, we need to calculate the noise and the signal of the detector. The noise current in both interband and intersubband photodetectors is $I_n = qg\sqrt{2V(G+R)\mathrm{BW}}$, where $V = A_e t$ is the electrical volume of the detector, A_e and t are the semiconductor area and thickness, g is the internal gain, and G and R are the generation and recombination rates. For a device operating near equilibrium, we have $G \cong R$. The net recombination rate is the sum of the radiative and non-radiative recombination rates: $R = R_{rad} + R_{non\text{-}rad}$. The photodetector signal or current responsivity is $R_i = \eta q g \lambda / hc$, where η is QE and λ is the wavelength of the light. The device detectivity (sensitivity) is the signal-to-noise ratio, normalized for area and bandwidth: $D^* = R_i / I_n \sqrt{A_0 \mathrm{BW}}$, where A_0 is the optical (collecting) area of the device. Assuming equal optical and electrical areas (*i.e.* conventional photodetectors), the optimum detector thickness is found to be $t_{opt} = 1.26/\alpha$, leading to the highest possible sensitivity of $D^*_{max} = 0.31\lambda/hc\sqrt{\alpha/R}$, where α is the semiconductor absorption coefficient.

This has been the sensitivity limit of conventional photodetectors for the past few decades. Further, we would like to see if optical antennas can help us exceed the above sensitivity limit. In this analysis, we assume that the beam is already focused to a diffraction-limited spot using conventional optics with an NA of ~1 (*i.e.* the practical focusing limit in the air). The optical area is then $A_0 \sim \lambda_0^2/\pi\mathrm{NA}$.

First, we find the detectivity of a deep sub-wavelength detector with volume $V \ll \lambda^3$ without any antennas to be $D_0^* \sim 0.5\alpha/hc\sqrt{\pi V/R}$. As expected, the detectivity degrades for smaller device volumes since the signal decreases at a faster pace than the noise.

Furthermore, we would like to see whether we can increase the QE and detectivity of a deep sub-wavelength detector using antennas. Since LDOS enhancement is highly dependent on the geometry and configuration of the antennas, it is not possible to develop a general formalism. Therefore, we will quantify this effect using two examples: a widely used bowtie antenna and a metallo-dielectric hybrid antenna we recently proposed.[12] The bowtie antenna does not produce a large QE and is not directional, while the hybrid antenna can produce a much higher QE and directivity. In both cases, electric field enhancement at the load site of antenna increases the optical absorption in the semiconductor. However, loading effect limits this enhancement as QE grows so that QE always stays below unity. In addition, we will see that the performance in each case strongly depends on whether an interband or an intersubband subwavelength detector is used.

Both antennas were optimized for detection at $\lambda = 8$ μm. The length of each bowtie's arm was 350 nm with 50 nm thickness. The hybrid antenna has a microsphere (inset of Fig. 7) with 20 μm diameter made of SiO_2. The detector dimension was 400 nm × 400 nm × 100 nm for the bowtie and 1 μm × 1.5 μm × 2 μm for the hybrid antenna. The real part of the semiconductor refractive index was assumed to be about 3, and the absorption coefficients were assumed to be 1000 cm^{-1} for the intersubband and 5000 cm^{-1} for the interband absorber.[73] Here, we assumed that doped semiconductor layers are used as the electric contacts to extract photogenerated carriers. As commonly used in photodiodes, an optimum doping level provides a small contact resistivity (compared with the device resistivity) while maintaining a negligible free-carrier absorption.

LDOS calculation in the presence of a lossy medium is not a well-defined problem and is an open subject for researchers (see section 2.2). In this paper, finite-difference time-domain (FDTD) method was used to calculate LDOS at the absorber site using the following:[17]

$$\mathrm{LDOS}_l(x_0, \omega) = \frac{4}{\pi}\varepsilon(x_0) P_l(x_0, \omega) \quad (4)$$

where $P_l(x_0, \omega)$ is the radiative power from a dipole that is placed at x_0 and has the polarization state l. Since the system is dissipative due to the optical absorption of the semiconductor, the radiative recombination can decay into a finite range of frequencies. Thus, the total LDOS is calculated by integrating the overall frequencies weighted by a Lorentzian lineshape for their contribution.[17]

$$\mathrm{LDOS}(x_0) = \int \frac{1}{\varepsilon(x_0)} \mathrm{LDOS}_l(x_0, \omega) \frac{\gamma_0/\pi}{(\omega - \omega_0)^2 + \gamma_0} \mathrm{d}\omega \quad (5)$$

This approach ensures that the non-radiative decay of dipole due to the dissipative host is considered by γ_0. The value of QE is calculated from the net power dissipated by the absorber, normalized to a Gaussian source with numerical aperture NA = 1 (corresponding to $A_0 \sim \lambda_0^2/\pi\mathrm{NA}$). Fig. 6 shows QE and LDOS enhancement as a function of distance r between the detector and the bowtie antenna gap. In this geometry, LDOS and QE monotonically increase as r approaches zero, signifying the optical antenna's role in enhancing the spontaneous emission and far-field power absorption in the semiconductor absorber. Although the bowtie antenna significantly enhances QE, the maximum value is still around 1%. Also, the bowtie directivity is quite dismal (~2 dB). On the contrary, the hybrid antenna can simultaneously produce a high QE of about 50% and a high directivity (~20 dB).[12]

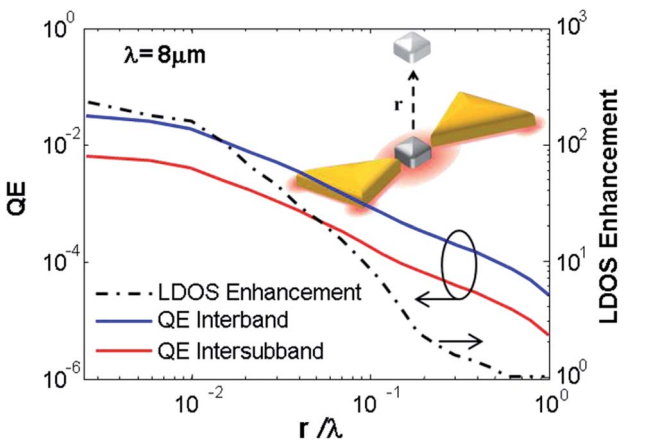

Fig. 6 LDOS enhancement and QE of subwavelength interband and intersubband absorbers with volume $V = 3.1 \times 10^{-5}\lambda^3$, as a function of distance r from the center of a bowtie designed for $\lambda = 8$ μm.

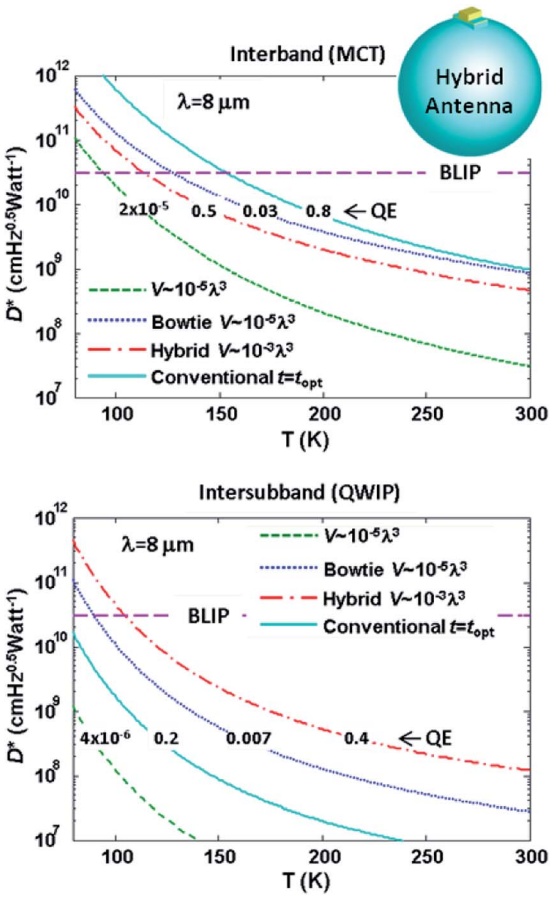

Fig. 7 Detectivity *versus* temperature for interband (top) and intersubband (bottom) absorbers. The plots compare detectivity and QE for four cases: a deep sub-wavelength absorber, bowtie and hybrid antennas integrated with sub-wavelength absorbers and a conventional detector with optimum thickness. Optical antennas dramatically enhance the detectivity of the intersubband devices and surpass the limit of conventional device by ~30 times, but their LDOS enhancement prevents detectivity improvement for the interband devices. The inset in the top figure is the geometry of hybrid antenna consisting of a microsphere antenna and a metallo-dielectric cavity antenna. Semiconductor detector is enclosed by the cavity.

We would also like to compare the detectivity of interband and intersubband detectors integrated with each antenna and compare them to the conventional values at $\lambda = 8$ μm. The main question is whether a high LDOS produced by the bowtie and hybrid antennas (~230 and 1100 times vacuum level, respectively) can adversely affect their detectivity due to the reduced radiative lifetime.

Fig. 7 shows the calculated detectivity for the above antennas for the two cases of interband and intersubband absorbers. For interband, we used the parameters[74] of $Hg_{1-x}Cd_xTe$ (MCT) with a cutoff wavelength of around 8 μm (x of ~0.22). For intersubband, we used the parameters[73] of AlGaAs QWIP with a peak detection wavelength of 8 μm. The background-limited performance (BLIP) detectivity is also shown in this figure. It is evident that the detectivity of hybrid antennas integrated with QWIP is more than 30 times higher than the limit of conventional QWIP detectors at all temperatures. In addition, QE of ~40% is also quite large. However, the optical antennas could not increase the detectivity of the interband detector beyond the limit of conventional devices because of the comparable radiative τ_{rad} and non-radiative lifetime $\tau_{non\text{-}rad}$ in interband detectors. For example, the ratio of the radiative to non-radiative lifetime in MCT is around 0.1 at $T = 77$ K and 25 at room temperature. However, LDOS enhancements of 230 for the bowtie antenna means that the new radiative recombination lifetime is about ten times smaller than the non-radiative lifetime even at room temperature. Therefore, the noise of the detector integrated with the antenna is dominated by the enhanced radiative noise at any temperature. However, for QWIP, $\tau_{rad} \sim 1$ μs and $\tau_{non\text{-}rad} \sim 200$ ps at $T = 77$ K,[75] and hence, the ratio is about 5000. This large ratio means that the LDOS enhancement, even for the hybrid antenna, cannot enhance the detector noise at any temperature. This conclusion is valid for the mid- and long-wavelength infrared interband and intersubband detectors (3 μm < λ < 12 μm). In the shorter wavelength bands, where intersubband detectors are not commonly used, their performance may be limited by the LDOS enhancement. In the very long-wavelength infrared (VLWIR) and terahertz (THz) region, where interband devices are not commonly used, LDOS enhancement will not produce the aforementioned limit. Therefore, this analysis suggests that optical antennas integrated with interband devices in these spectral bands have a lot of unexplored potential. Let us now look at the state-of-the-art in each interband and intersubband category.

3.3.1. Optical antennas integrated with interband photodetector. In a pioneering work, Tang *et al.* reported a metal–semiconductor–metal (MSM) germanium (Ge) detector with a deep sub-wavelength dimension ~λ^3/10 000 integrated with a half-wave Hertz dipole antenna.[9] The extremely small volume suggests a high speed operation of ~100 GHz as well as a very small capacitance. The latter is particularly important as a large load resistance can be used to generate a high output voltage and very low optical and electrical power consumption for on-chip optical interconnects. The performance enhancement of MSM photodetectors has been the subject of much research[76–83] due to their relative low cost of fabrication and compatibility with CMOS technology.[76] The detector's electrodes, used for extracting the current, can serve as optical antennas to capture and focus light efficiently at the detection site. For example, Ren *et al.* reported an integration of a split-ring bull's eye antenna on a germanium detector.[78] The bull's eye antenna focuses light from a relatively large area (with a diameter of ~10 λ) into a subwavelength germanium slab, resulting in an enhancement of the LDOS and electric field. The measured photocurrent is improved by a factor of 7 with a responsivity of ~3.93 μA W^{-1}. Fan *et al.* have fabricated the electrodes of a germanium nanowire to capture light from the far-field and concentrate it on the germanium nanowire.[77] The nanowire has optical resonant modes that can coincide with the contact antenna's resonance wavelength resulting in ~1.7 times enhancement of polarization-dependent optical absorption in germanium at 660 nm wavelength. Combining a resonant microcavity with an optical antenna increases the photon interaction time at the

detection site, in addition to the efficiency of the far-field to near-field coupling. K. Balram *et al.* have reported a hybrid micro-cavity optical antenna that strongly enhances the optical absorption in a germanium detector below the band gap with a measured responsivity of ~1.2 A W^{-1}. The microcavity antenna consists of a planar metal–dielectric resonant cavity.[76] The electrodes adjacent to the germanium create a cavity in the germanium region. The cavity size (germanium width) is tailored in order to excite the highest Q mode (5th cavity mode) to increase the photon interaction time in the cavity. In addition, changing the germanium's width will shift the wavelength of the cavity mode, which changes the detection wavelength, adding a tuning feature to the detector. The same group has reported a similar structure with a MSM deep sub-wavelength silicon photodetector operating at the near-IR region.[80] The demonstrated MSM silicon photodetector has the tuning feature due to the microcavity antenna, which is favourable for applications, such as multispectral imaging sensors and short-range optical interconnects.

3.3.2. Optical antennas integrated with intersubband photodetector. Photodetectors based on the intersubband absorption of photons in quantum wells have two distinct features when compared with interband detectors: a high non-radiative recombination rate due to the fast LO phonon scattering between the subbands and high polarization sensitivity due to the quantum well transition selection rule. Since quantum wells are usually separated by rather thick barriers and a relatively small dipole matrix, the overall optical absorption coefficient of intersubband detectors is considerably smaller than interband detectors. The shorter carrier lifetime and smaller optical absorption coefficient means that the detectivity of intersubband detectors is fundamentally lower than that of interband detectors. However, the technological advantages of intersubband detectors have made them an attractive choice for many applications— particularly at the longer infrared wavelength range. As we discussed in section 3.3, the effect of optical antennas is more significant for intersubband mid- and long-wavelength infrared photodetectors, where the weak optical absorption results in a QE of about 20% in conventional devices. In 2010, we reported[10] an ultra-thin (λ/16) QWIP integrated with a nanohole-array optical antenna to produce a high QE of ~40% (see Fig. 8a and b). The top view of the $|E_z|^2$ at the nanohole-array/detector interference and simulated with FDTD as well as the side view of $|E_z|^2$ through the quantum well's growth direction are shown in Fig. 8c and d. The responsivity and detectivity of this device are shown in Fig. 8e. The optical antenna captures far-field light and enhances its concentration at the active region of QWIP. In addition, QWIP can only absorb light with a polarization perpendicular to the growth direction. The nanohole-array antenna converts the lateral polarization of light to a perpendicular polarization by exciting the surface plasmons on the surface of the perforated metal. Fig. 5b shows the simulated electric intensity with a polarization perpendicular to the QW growth direction. The peaks of responsivity and detectivity both occur at 8 μm, reaching ~7 A W^{-1} and ~7.4 × 10^{10} cm $Hz^{1/2}$ per W, respectively. A similar far-field to near-field coupling property of

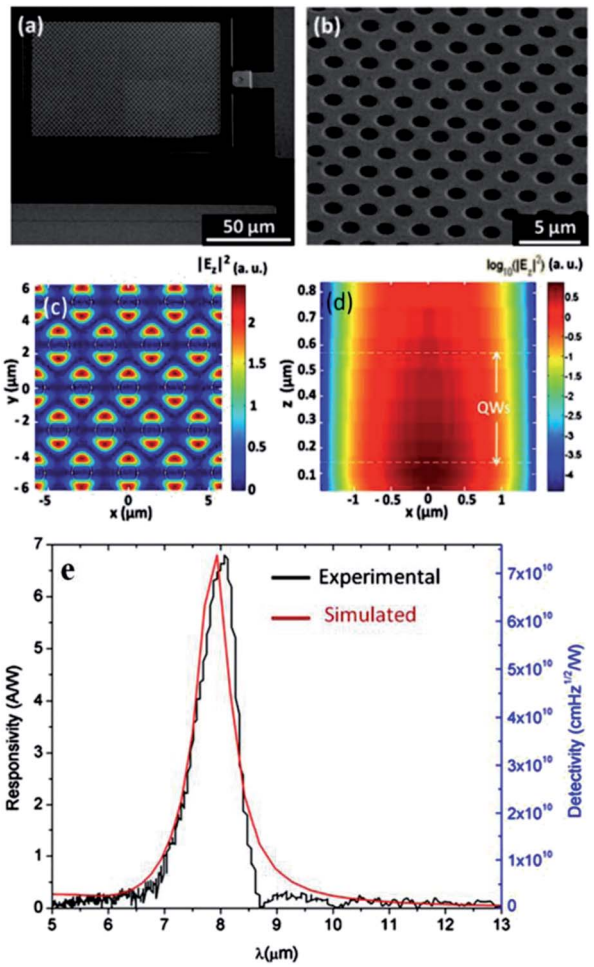

Fig. 8 (a) SEM images of nanohole array optical antenna integrated on a QWIP photodetector. (b) Map of FDTD simulated $|E_z|^2$ at the bottom of nanohole array antenna, (c) along the quantum well's growth direction. (d) The measured responsivity of the device at bias 0.7 V at 78 K and the spectrum of average $|E_z|^2$ in the active region. Reproduced with permission of the American Institute of Physics from ref. 10.

periodic hole arrays has been reported without using surface plasmons. In this work, QWIP operating at 7.6 μm was integrated with a hexagonal air-hole array. Although a similarly high enhancement could be produced with this microresonator photonic crystal QWIP, the high Q factor of about 135 led to an extremely narrow detection bandwidth.[84]

Nanohole array optical antennas have been used to enhance quantum dot infrared photodetectors (QDIPs)[85] as well, with about five times enhancement in the responsivity and the detectivity. In addition, a focal plane array (FPA) of nanohole optical antennas integrated on a QDIP has been reported with 15 times greater detectivity at 8.3 μm wavelength.[86]

Although, nanohole array antenna enhances the photodetector performance, it only confines light in one dimension. Similar to the MSM Ge integration with microcavity antenna, incorporation of microcavity property with far-field to near-field coupling can increase the light-matter interaction as well as allows reducing the detection volume in deep sub-wavelength scale. Recently, a double-metal nanoantenna as microcavity has

been fabricated on a QWIP detector to 3-dimensionally confine light.[87] Strong sub-wavelength light confinement of this microcavity antenna leads to three times reduction in dark current due to the reduced detection area. As described in section 3.3, we recently proposed a novel hybrid optical antenna[12] that can achieve a similarly higher QE, but at smaller volumes. In addition, it can produce a large directivity. The simulated QE is ~50% and directivity gain of ~16 dB has been achieved in a QWIP active region with a volume of ~0.006 λ^3. A recent simulation of another type of metallo-dielectric optical antenna[88] suggests that large QE of over 85% with extremely large emission rate enhancements of LDOS ~3000 is possible for single dipole emitter/absorber.

3.3.3. Direct detection optical antennas. In the direct detection, optical antenna not only enhances coupling to free-space electromagnetic waves, but also plays a central role in the conversion of electromagnetic waves to electrical signals. Here, we discuss two important direct detection antennas: the rectenna, which is based on electronic rectification of optical field and the Schottky diode optical antenna, which is based on the photoemission process from the antenna to a semiconductor. In the latter, a cut-off frequency exists due to the quantum barrier, whereas in the former, the process of optical to electrical conversion is not limited by incident photon energy.

3.3.3.1. Infrared rectenna. A rectifying antenna, or so-called rectenna, is a combination of a receiving nanoantenna and a diode that can convert optical power to electrical signal by rectifying the AC current induced in the antenna. Rectification of the optical single with GHz and THz frequencies can be achieved by semiconductor electronics, such as CMOS transistors,[89] whereas optical signals in infrared and higher frequencies cannot be rectified by semiconductors due to their relative slow switching speed. The rectification process in the infrared and visible regions are based on a metal–oxide–metal (MOM) diode through the fast process of electron tunneling.[90] The concept of the rectenna originated from the whisker diodes[91] in the 1960s for millimeter wave frequency conversion and multiplication applications. The first efficient rectenna consisted of a $\lambda/2$ dipole antenna with a point contact, which was placed $\lambda/4$ above a reflecting plane.[92] Later, Wilke *et al.* developed a 30 THz rectenna consisting of a half-wave dipole antenna and a MOM diode.[93] The optical antenna part of a rectenna plays several roles.[90] It couples the far-field radiation into a tiny volume of the rectifier leading to very fast response. In addition, optical antenna's response can be tuned to a specific frequency, primarily based on the geometry and independent of materials. Unfortunately, the contrast between the resistance of a good rectifier and an antenna's impedance is typically several orders of magnitude, imposing poor impedance matching.[94] Based on circuit theory, the maximum power transferred to the load happens when the load's impedance is the conjugate of the antenna's impedance. Based on Fano,[95] there is a fundamental limitation in impedance matching, which results in a tradeoff between the operating bandwidth and transferred power to the load in this case. Another obstacle in a rectenna is the fill-factor of the antenna in each pixel of a focal plane array (FPA).[90] Due to the electrically small size of a metallic antenna, its optical cross-section is much smaller than the host pixel area. In addition, the far-field power that reaches each detector pixel is very small due to the incoherent nature of the incoming signal. Therefore, diffractive optical elements, such as the Fresnel zone plate lens[96] as well as the hybrid optical antenna[97] could be used to compensate the low fill-factor and inefficient far-field power collection of the antenna.

3.3.3.2. Antenna Schottky detector. Schottky detectors are based on the optical excitation of electrons in metals (*i.e.* antenna) and their subsequent thermionic emission to another layer[5] (usually a semiconductor). In 1973, Shepherd and Yang proposed the idea of Schottky detector arrays as infrared imaging sensors.[98] Within a few years, the first Schottky infrared CCD imagers based on thin palladium/platinum on silicon[99] were realized. Although many semiconductors, such as HgCdTe are capable of absorbing light at the infrared and longer wavelengths, these materials are expensive and difficult to work with. However, a few nanometers of metal on silicon can produce optical absorption beyond the band gap of the silicon, leading to the detection of short-, mid-, and long-wavelength infrared. This type of Schottky detector is highly compact and compatible with CMOS technology and favorable for integration with silicon photonics. The main drawback in the Schottky detector is its low responsivity (less than 100 $\mu A\ W^{-1}$) due to inefficient electron emission across the barrier as well as low optical absorption within the electron diffusion thickness of the metal.[100]

Although the surface plasmon decay on a metal surface is considered as a limiting factor in plasmonic device performance, it has the ability to generate hot electrons[100,101] that can be used in photocatalysis,[102] photovoltaics,[103] and photodetectors.[5] The hot electrons generated by plasmonic decay in a metal could possess enough momentum to traverse a Schottky barrier.[104] Unprecedented Schottky detector responsivity has recently been achieved by integration with optical antennas, such as a metal grating with the ability to tune the responsivity peak,[101] a 5 nm embedded 3D junction with 25 times enhancement of responsivity over planar diodes,[104] a deep trench cavity array,[35] and a metamaterial perfect absorber[100] with the capability of broadband and polarization insensitive responses.

3.3.4. Optical antennas integrated with two-dimensional semiconductor photodetectors. Another emerging photon detection platform is the two-dimensional system. The most notable material is graphene, which is a monoatomic layer of carbon atoms in a hexagonal honeycomb arrangement. The high mobility, tunability, and broadband absorption of graphene makes it very attractive for ultrafast photodetectors.[105,106] Unfortunately, graphene has a very small absorption cross section (~2.3% absorption in visible and infrared regions) that significantly limits the QE of graphene-based photodetectors compared with III–V based photodetectors.[107,108] To address this limitation, various optical antennas have recently been integrated with graphene photodetectors.[106,108–111] Integration with optical antennas keeps the properties of graphene intact while improving QE. For example, Z. Fang *et al.* utilized an optical antenna sandwiched between two graphene monolayers,

resulting in 800% enhancement of photocurrent, with 20% internal quantum efficiency.[109] They showed that an optical antenna enhances intrinsic absorption of graphene as well as transferring hot electrons from the antenna to the graphene. T. J. Echtermeyer *et al.* demonstrated a 20 times QE enhancement of a graphene-based p–n photodetector integrated with an optical antenna, due to the field enhancement across the junction.[108] In addition to light–matter interaction enhancement, the combination of optical antennas and graphene can add tunability to the photodetector response through electrostatic gating of graphene.[110,112–114] Another interesting feature of optical antennas integrated with graphene is the ability to electrically read out the optical field at nanoscale regions due to the inherent nanoscale dimensions of graphene photodetector. S. Shi *et al.* demonstrated a bowtie antenna combined with a nano-constricted graphene layer using a two-step electromigration process.[115] This device achieved an electric field enhancement up to 100 times.

Recently, graphene-like 2D materials, or the so-called van der Waals materials, have attracted many researchers due to their distinguished optical and electronic properties compared with graphene. Unlike the zero-gap graphene, some of the 2D materials, such as layered metal chalcogenides are semiconductors with direct and indirect energy band gaps. Examples of recent 2D materials are MoS_2, GaS, GaSe, GaTe, WS_2, and hexagonal boron nitride (h-BN) nanosheets.[116] Very recently, the optical properties of a MoS_2/Ag nanowire antennas was investigated.[117] In this work, a coupling between single-layer MoS_2 and a single Ag nanowire has been demonstrated, which resulted in direct plasmon-to-exciton conversion along the Ag nanowire antenna to serve a dual role: both to excite MoS_2 and to extract the decaying MoS_2 excitons. Similar excitation transfer has been investigated between Au nanoparticles and MoS_2.[118] These works are important steps in incorporating optical antennas with 2D materials.

4. Conclusion

In this paper, we reviewed the recent progress and developments in optical antennas integrated with active optoelectronic devices, such as lasers, LEDs, and photodetectors. Theoretical and experimental works suggest that such devices have the potential to address many of the inherent limitations of conventional optoelectronic devices. In particular, they have two significant capabilities. They can enhance both the local density of states and the coupling of the near-field modes to the far-field modes. Many devices utilizing these capabilities to achieve enhanced efficiency and sensitivity have successfully been demonstrated. However, the enhancement of the light–matter interaction does not necessarily lead to increased sensitivity. We showed that the sensitivity of detectors could even degrade with the addition of optical antennas, if their noise is already limited by the radiative generation of carriers.

Historically, the strong light–matter coupling produced by optical cavities in the field of cavity quantum electrodynamics (CQED), has led to significant fundamental and practical discoveries,[119] as signified by the 2012 Nobel Prize in Physics. However, the required high quality factor of such cavities makes it difficult to achieve a fast interaction time. On the contrary, optical antennas have the ability to enhance the light–matter coupling at nano-scale dimensions and at ultrafast time scales.[120] These unique abilities could potentially lead to significant fundamental and practical breakthroughs. Recent experimental demonstrations, such as ultrafast optical spectroscopy of nanoparticles[121] and nano-spectroscopic imaging[122] suggest that rapid progress in this field has already started. In parallel, the unique properties of optical antennas have excellent synergy with the properties new 1D and 2D active devices, such as carbon nanotube and graphene. Early demonstrations in this area[123–125] are indicative of a paradigm shift in the field of nano-optoelectronics. On a broader scale, we believe that the impact of integrated optical antennas on many technologies, including ultra-sensitive compact medical sensors and ultrafast on-chip optical interconnects is imminent.

Acknowledgements

This work is partially supported by ARO through award #W911NF-11-1-0390, and NSF through award # ECCS-1206155 and # ECCS-1310620.

References

1 A. Kinkhabwala, Z. Yu, S. Fan, Y. Avlasevich, K. Müllen and W. Moerner, *Nat. Photonics*, 2009, **3**, 654–657.
2 N. Liu, M. L. Tang, M. Hentschel, H. Giessen and A. P. Alivisatos, *Nat. Mater.*, 2011, **10**, 631–636.
3 J. B. Lassiter, H. Sobhani, J. A. Fan, J. Kundu, F. Capasso, P. Nordlander and N. J. Halas, *Nano Lett.*, 2010, **10**, 3184–3189.
4 N. Liu, L. Langguth, T. Weiss, J. Kästel, M. Fleischhauer, T. Pfau and H. Giessen, *Nat. Mater.*, 2009, **8**, 758–762.
5 M. W. Knight, H. Sobhani, P. Nordlander and N. J. Halas, *Science*, 2011, **332**, 702–704.
6 K. Ding and C. Ning, *Light: Sci. Appl.*, 2012, **1**, e20.
7 N. Yu, P. Genevet, F. Aieta, M. Kats, R. Blanchard, G. Aoust, J. Tetienne, Z. Gaburro and F. Capasso, *IEEE Journal of Selected Topics in Quantum Electronics*, 2013, 4700423.
8 H. Chen, C. Chan and P. Sheng, *Nat. Mater.*, 2010, **9**, 387–396.
9 L. Tang, S. E. Kocabas, S. Latif, A. K. Okyay, D.-S. Ly-Gagnon, K. C. Saraswat and D. A. Miller, *Nat. Photonics*, 2008, **2**, 226–229.
10 W. Wu, A. Bonakdar and H. Mohseni, *Appl. Phys. Lett.*, 2010, **96**, 161107–161103.
11 A. Bonakdar, J. Kohoutek, D. Dey and H. Mohseni, *Opt. Lett.*, 2012, **37**, 3258–3260.
12 A. Bonakdar and H. Mohseni, *Opt. Lett.*, 2013, **38**, 2726–2728.
13 M. Agio, *Nanoscale*, 2012, **4**, 692–706.
14 L. Yousefi and A. C. Foster, *Opt Express*, 2012, **20**, 18326–18335.
15 A. Ahmed and R. Gordon, *Nano Lett.*, 2012, **12**, 2625–2630.
16 A. F. Koenderink, *Opt. Lett.*, 2010, **35**, 4208–4210.

17 A. Taflove, S. G. Johnson and A. Oskooi, *Advances in FDTD Computational Electrodynamics: Photonics and Nanotechnology*, Artech house, 2013.
18 S. Scheel, L. Knoll and D. G. Welsch, *Phys. Rev. A*, 1999, **60**, 4094–4104.
19 S. M. Barnett, B. Huttner and R. Loudon, *Phys. Rev. Lett.*, 1992, **68**, 3698–3701.
20 H. T. Dung, L. Knoll and D. G. Welsch, *Phys. Rev. A*, 2000, **62**, 053804.
21 G. Juzeliunas, *Phys. Rev. A*, 1997, **55**, R4015–R4018.
22 S. Scheel, L. Knoll, D. G. Welsch and S. M. Barnett, *Phys. Rev. A*, 1999, **60**, 1590–1597.
23 M. S. Tomas and Z. Lenac, *Phys. Rev. A*, 1997, **56**, 4197–4206.
24 M. S. Tomas and Z. Lenac, *Phys. Rev. A*, 1999, **60**, 2431–2437.
25 G. C. des Francs, C. Girard, J. C. Weeber, C. Chicane, T. David, A. Dereux and D. Peyrade, *Phys. Rev. Lett.*, 2001, **86**, 4950–4953.
26 C. Sauvan, J. P. Hugonin, I. S. Maksymov and P. Lalanne, *Phys. Rev. Lett.*, 2013, **110**, 237401.
27 C. Van Vlack and S. Hughes, *Opt. Lett.*, 2012, **37**, 2880–2882.
28 N. Engheta, A. Salandrino and A. Alu, *Phys. Rev. Lett.*, 2005, **95**, 095504.
29 N. Engheta, *Science*, 2007, **317**, 1698–1702.
30 D. W. Beekman and J. B. Van Anda, Polarization-sensitive QWIP thermal imager, *Proc. SPIE, Infrared Detectors and Focal Plane Arrays VI*, 2000, **4028**, 102.
31 F. Cremer, P. B. Schwering, W. de Jong, K. Schutte and A. N. de Jong, *Proc. SPIE, Atmospheric Propagation and Remote Sensing IV*, 1995, **2471**, 204.
32 T. W. Cronin, N. Shashar, R. L. Caldwell, J. Marshall, A. G. Cheroske and T.-H. Chiou, *Integr. Comp. Biol.*, 2003, **43**, 549–558.
33 F. Meriaudeau, M. Ferraton, C. Stolz, O. Morel and L. Bigué, Polarization imaging for industrial inspection, *Proc. SPIE*, 2008, **6813**, 681308-1.
34 D. Okamoto, J. Fujikata and K. Ohashi, *Jpn. J. Appl. Phys.*, 2011, **50**, 120201.
35 K.-T. Lin, H.-L. Chen, Y.-S. Lai and C.-C. Yu, *Nat. Commun.*, 2014, **5**, 3288.
36 A. Partovi, D. Peale, M. Wuttig, C. A. Murray, G. Zydzik, L. Hopkins, K. Baldwin, W. S. Hobson, J. Wynn, J. Lopata, L. Dhar, R. Chichester and J. H.-J. Yeh, *Appl. Phys. Lett.*, 1999, **75**, 1515–1517.
37 F. Chen, A. Itagi, J. Bain, D. Stancil, T. Schlesinger, L. Stebounova, G. Walker and B. Akhremitchev, *Appl. Phys. Lett.*, 2003, **83**, 3245–3247.
38 B. Guo, G. Song and L. Chen, *J. Opt. A: Pure Appl. Opt.*, 2008, **10**, 085202.
39 H. Gai, J. Wang, Q. Tian, W. Xia and X. Xu, *J. Opt. A: Pure Appl. Opt.*, 2007, **9**, 998.
40 J.-x. Gao, G.-f. Song, Q.-q. Gan, B. Guo and L. Chen, *Laser Phys. Lett.*, 2007, **4**, 234–237.
41 B. Guo, G. Song and L. Chen, *Appl. Phys. Lett.*, 2007, **91**, 021103.
42 Z. Rao, L. Hesselink and J. S. Harris, *Opt. Express*, 2007, **15**, 10427–10438.
43 N. Yu, J. Fan, Q. J. Wang, C. Pflügl, L. Diehl, T. Edamura, M. Yamanishi, H. Kan and F. Capasso, *Nat. Photonics*, 2008, **2**, 564–570.
44 N. Yu, R. Blanchard, J. Fan, F. Capasso, T. Edamura, M. Yamanishi and H. Kan, *Appl. Phys. Lett.*, 2008, **93**, 181101.
45 J. Tetienne, R. Blanchard, N. Yu, P. Genevet, M. Kats, J. Fan, T. Edamura, S. Furuta, M. Yamanishi and F. Capasso, *New J. Phys.*, 2011, **13**, 053057.
46 N. Yu, M. Kats, C. Pflugl, M. Geiser, Q. J. Wang, M. A. Belkin, F. Capasso, M. Fischer, A. Wittmann and J. Faist, *Appl. Phys. Lett.*, 2009, **95**, 161108.
47 R. Blanchard, T. S. Mansuripur, B. Gokden, N. Yu, M. Kats, P. Genevet, K. Fujita, T. Edamura, M. Yamanishi and F. Capasso, *Appl. Phys. Lett.*, 2013, **102**, 191114.
48 Y. Nanfang, W. Qi Jie, C. Pflugl, L. Diehl, F. Capasso, T. Edamura, S. Furuta, M. Yamanishi and H. Kan, *Appl. Phys. Lett.*, 2009, **94**, 151101.
49 N. Yu, Q. J. Wang, M. A. Kats, J. A. Fan, S. P. Khanna, L. Li, A. G. Davies, E. H. Linfield and F. Capasso, *Nat. Mater.*, 2010, **9**, 730–735.
50 G. Liang, H. Liang, Y. Zhang, S. P. Khanna, L. Li, A. Giles Davies, E. Linfield, D. Fatt Lim, C. Seng Tan and S. Fung Yu, *Appl. Phys. Lett.*, 2013, **102**, 031119.
51 E. Cubukcu, E. A. Kort, K. B. Crozier and F. Capasso, *Appl. Phys. Lett.*, 2006, **89**, 093120.
52 X. Shi and L. Hesselink, *Jpn. J. Appl. Phys.*, 2002, **41**, 1632.
53 N. Yu, E. Cubukcu, L. Diehl, M. A. Belkin, K. B. Crozier, F. Capasso, D. Bour, S. Corzine and G. Hofler, *Appl. Phys. Lett.*, 2007, **91**, 173113.
54 D. Dey, J. Kohoutek, R. M. Gelfand, A. Bonakdar and H. Mohseni, *Opt. Lett.*, 2010, **35**, 2783–2785.
55 D. Dey, J. Kohoutek, R. M. Gelfand, A. Bonakdar and H. Mohseni, *IEEE Photonics Technol. Lett.*, 2010, **22**, 1580–1582.
56 D. Austin, N. Mullin, I. Luxmoore, I. Sandall, A. Cullis, A. Bismuto, J. Faist, J. Hobbs and L. Wilson, *Appl. Phys. Lett.*, 2010, **96**, 151105.
57 D. Austin, N. Mullin, A. Bismuto, I. Luxmoore, A. Adawi, D. Revin, M. Soulby, J. Cockburn, Q. Jiang and A. Krysa, *IEEE Photonics Technol. Lett.*, 2010, **22**, 1217–1219.
58 N. Yu, E. Cubukcu, L. Diehl, D. Bour, S. Corzine, J. Zhu, G. Höfler, K. B. Crozier and F. Capasso, *Opt. Express*, 2007, **15**, 13272–13281.
59 R. M. Gelfand, D. Dey, J. Kohoutek, A. Bonakdar, S. C. Hur, D. D. Carlo and H. Mohseni, *Opt. Photonics News*, 2011, **22**, 32–37.
60 J. Kohoutek, D. Dey, A. Bonakdar, R. Gelfand, V. Fathipour, O. G. Memis and H. Mohseni, *Small*, 2012, **8**, 3781–3785.
61 Q. Qin, B. S. Williams, S. Kumar, J. L. Reno and Q. Hu, *Nat. Photonics*, 2009, **3**, 732–737.
62 J. Kohoutek, A. Bonakdar, R. Gelfand, D. Dey, I. Hassani Nia, V. Fathipour, O. G. Memis and H. Mohseni, *Nano Lett.*, 2012, **12**, 2537–2541.
63 P. Dawson, D. Walmsley, H. Quinn and A. Ferguson, *Phys. Rev. B: Condens. Matter Mater. Phys.*, 1984, **30**, 3164.

64 K. Okamoto, I. Niki, A. Shvartser, Y. Narukawa, T. Mukai and A. Scherer, *Nat. Mater.*, 2004, **3**, 601–605.
65 A. Kock, E. Gornik, M. Hauser and W. Beinstingl, *Appl. Phys. Lett.*, 1990, **57**, 2327–2329.
66 J. Vuckovic, M. Loncar and A. Scherer, *IEEE J. Quantum Electron.*, 2000, **36**, 1131–1144.
67 D. Arbel, N. Berkovitch, A. Nevet, A. Peer, S. Cohen, D. Ritter and M. Orenstein, *Opt. Express*, 2011, **19**, 9807–9813.
68 S. Mokkapati, D. Saxena, H. H. Tan and C. Jagadish, *Small*, 2013, **9**, 3964–3969.
69 C.-Y. Cho, Y. Zhang, E. Cicek, B. Rahnema, Y. Bai, R. McClintock and M. Razeghia, *Appl. Phys. Lett.*, 2013, **102**, 211110.
70 A. Boltasseva and H. A. Atwater, *Science*, 2011, **331**, 290–291.
71 A. Dentai, R. Kuchibhotla, J. Campbell, C. Tsai and C. Lei, *Electron. Lett.*, 1991, **27**, 2125–2127.
72 K. Kishino, M. S. Unlu, J.-I. Chyi, J. Reed, L. Arsenault and H. Morkoc, *IEEE J. Quantum Electron.*, 1991, **27**, 2025–2034.
73 A. Rogalski, *Prog. Quantum Electron.*, 2003, **27**, 59–210.
74 V. Lopes, A. Syllaios and M. Chen, *Semicond. Sci. Technol.*, 1993, **8**, 824.
75 A. Rogalski, *J. Appl. Phys.*, 2003, **93**, 4355–4391.
76 K. C. Balram, R. M. Audet and D. A. Miller, *Opt. Express*, 2013, **21**, 10228–10233.
77 P. Fan, K. C. Huang, L. Cao and M. L. Brongersma, *Nano Lett.*, 2013, **13**, 392–396.
78 F.-F. Ren, K.-W. Ang, J. Ye, M. Yu, G.-Q. Lo and D.-L. Kwong, *Nano Lett.*, 2011, **11**, 1289–1293.
79 T. J. Seok, A. Jamshidi, M. Eggleston and M. C. Wu, *Opt. Express*, 2013, **21**, 16561–16569.
80 K. C. Balram and D. A. Miller, *Opt. Express*, 2012, **20**(20), 22735–22742.
81 J. K. Hyun and L. J. Lauhon, *Nano Lett.*, 2011, **11**, 2731–2734.
82 L. Cao, J.-S. Park, P. Fan, B. Clemens and M. L. Brongersma, *Nano Lett.*, 2010, **10**, 1229–1233.
83 S. Collin, F. Pardo, N. Bardou, A. Lemaître, S. Averin and J.-L. Pelouard, *Opt. Express*, 2011, **19**, 17293–17297.
84 S. Kalchmair, R. Gansch, S. Ahn, A. Andrews, H. Detz, T. Zederbauer, E. Mujagić, P. Reininger, G. Lasser and W. Schrenk, *Opt. Express*, 2012, **20**, 5622–5628.
85 R. V. Shenoi, J. Rosenberg, T. E. Vandervelde, O. J. Painter and S. Krishna, *IEEE J. Quantum Electron.*, 2010, **46**, 1051–1057.
86 S. Lee, S. Krishna and S. Brueck, *IEEE Photonics Technol. Lett.*, 2011, **23**, 935–937.
87 Y. Nga Chen, Y. Todorov, B. Askenazi, A. Vasanelli, G. Biasiol, R. Colombelli and C. Sirtori, *Appl. Phys. Lett.*, 2014, **104**, 031113.
88 X. W. Chen, M. Agio and V. Sandoghdar, *Phys. Rev. Lett.*, 2012, **108**, 233001.
89 F. Schuster, D. Coquillat, H. Videlier, M. Sakowicz, F. Teppe, L. Dussopt, B. Giffard, T. Skotnicki and W. Knap, *Opt. Express*, 2011, **19**, 7827–7832.
90 J. Alda, J. M. Rico-García, J. M. López-Alonso and G. Boreman, *Nanotechnology*, 2005, **16**, S230.
91 L. O. Hocker, D. R. Sokoloff, V. Daneu, A. Szoke and A. Javan, *Appl. Phys. Lett.*, 1968, **12**, 401–402.
92 J. O. McSpadden, L. Fan and K. Chang, *IEEE Trans. Microwave Theory Tech.*, 1998, **46**, 2053–2060.
93 I. Wilke, Y. Oppliger, W. Herrmann and F. Kneubühl, *Appl. Phys. A: Solids Surf.*, 1994, **58**, 329–341.
94 M. Gadalla, M. Abdel-Rahman and A. Shamim, *Sci. Rep.*, 2014, **4**, 4270.
95 R. M. Fano, *J. Franklin Inst.*, 1950, **249**, 57–83.
96 F. J. Gonzalez, J. Alda, B. Ilic and G. D. Boreman, *Appl. Opt.*, 2004, **43**, 6067–6073.
97 A. Bonakdar and H. Mohseni, Hybrid optical antenna with high directivity gain, *Optics Letters*, 2013, **15**, 2726–2728.
98 F. Shepherd Jr and A. C. Yang, Silicon Schottky retinas for infrared imaging, *Electron Devices Meeting, 1973 International; IEEE*, 1973, 310–313.
99 W. F. Kosonocky, F. V. Shallcross, T. S. Villani and J. V. Groppe, *IEEE Trans. Electron Devices*, 1985, **32**, 1564–1573.
100 W. Li and J. G. Valentine, *Nano Lett.*, 2014, 3510–3514.
101 A. Sobhani, M. W. Knight, Y. Wang, B. Zheng, N. S. King, L. V. Brown, Z. Fang, P. Nordlander and N. J. Halas, *Nat. Commun.*, 2013, **4**, 1643.
102 J. Li, S. K. Cushing, P. Zheng, F. Meng, D. Chu and N. Wu, *Nat. Commun.*, 2013, **4**, 2651.
103 E. W. McFarland and J. Tang, *Nature*, 2003, **421**, 616–618.
104 M. W. Knight, Y. Wang, A. S. Urban, A. Sobhani, B. Y. Zheng, P. Nordlander and N. J. Halas, *Nano Lett.*, 2013, **13**, 1687–1692.
105 A. Grigorenko, M. Polini and K. Novoselov, *Nat. Photonics*, 2012, **6**, 749–758.
106 Y. Liu, R. Cheng, L. Liao, H. Zhou, J. Bai, G. Liu, L. Liu, Y. Huang and X. Duan, *Nat. Commun.*, 2011, **2**, 579.
107 Z. Sun and H. Chang, *ACS Nano*, 2014, 4133–4156.
108 T. Echtermeyer, L. Britnell, P. Jasnos, A. Lombardo, R. Gorbachev, A. Grigorenko, A. Geim, A. Ferrari and K. Novoselov, *Nat. Commun.*, 2011, **2**, 458.
109 Z. Fang, Z. Liu, Y. Wang, P. M. Ajayan, P. Nordlander and N. J. Halas, *Nano Lett.*, 2012, **12**, 3808–3813.
110 Y. Yao, M. A. Kats, R. Shankar, Y. Song, J. Kong, M. Loncar and F. Capasso, *Nano Lett.*, 2013, **14**, 214–219.
111 Z. Fang, Y. Wang, Z. Liu, A. Schlather, P. M. Ajayan, F. H. Koppens, P. Nordlander and N. J. Halas, *ACS Nano*, 2012, **6**, 10222–10228.
112 J. Kim, H. Son, D. J. Cho, B. Geng, W. Regan, S. Shi, K. Kim, A. Zettl, Y.-R. Shen and F. Wang, *Nano Lett.*, 2012, **12**, 5598–5602.
113 Y. Yao, M. A. Kats, P. Genevet, N. Yu, Y. Song, J. Kong and F. Capasso, *Nano Lett.*, 2013, **13**, 1257–1264.
114 N. K. Emani, T.-F. Chung, X. Ni, A. V. Kildishev, Y. P. Chen and A. Boltasseva, *Nano Lett.*, 2012, **12**, 5202–5206.
115 S.-F. Shi, X. Xu, D. Ralph and P. McEuen, *Nano Lett.*, 2011, **11**, 1814–1818.
116 O. Lopez-Sanchez, D. Lembke, M. Kayci, A. Radenovic and A. Kis, *Nat. Nanotechnol.*, 2013, **8**, 497–501.
117 K. M. Goodfellow, R. Beams, C. Chakraborty, L. Novotny and A. N. Vamivakas, arXiv preprint arXiv:1404.1853, 2014.
118 U. Bhanu, M. R. Islam, L. Tetard and S. Khondaker, arXiv preprint arXiv:1404.5645, 2014.

119 H. Walther, B. T. H. Varcoe, B. G. Englert and T. Becker, *Rep. Prog. Phys.*, 2006, **69**, 1325–1382.
120 D. Brinks, M. Castro-Lopez, R. Hildner and N. F. van Hulst, *Proc. Natl. Acad. Sci. U. S. A.*, 2013, **110**, 18386–18390.
121 T. Schumacher, K. Kratzer, D. Molnar, M. Hentschel, H. Giessen and M. Lippitz, *Nat. Commun.*, 2011, **2**, 333.
122 W. Bao, M. Melli, N. Caselli, F. Riboli, D. S. Wiersma, M. Staffaroni, H. Choo, D. F. Ogletree, S. Aloni, J. Bokor, S. Cabrini, F. Intonti, M. B. Salmeron, E. Yablonovitch, P. J. Schuck and A. Weber-Bargioni, *Science*, 2012, **338**, 1317–1321.
123 J. N. Chen, M. Badioli, P. Alonso-Gonzalez, S. Thongrattanasiri, F. Huth, J. Osmond, M. Spasenovic, A. Centeno, A. Pesquera, P. Godignon, A. Z. Elorza, N. Camara, F. J. G. de Abajo, R. Hillenbrand and F. H. L. Koppens, *Nature*, 2012, **487**, 77–81.
124 Y. Yao, M. A. Kats, P. Genevet, N. F. Yu, Y. Song, J. Kong and F. Capasso, *Nano Lett.*, 2013, **13**, 1257–1264.
125 X. M. W. L. Shao, H. T. Xu, J. F. Wang, J.-B. Xu, L.-M. Peng and H.-Q. Lin, *Adv. Opt. Mater.*, 2014, **2**, 162–170.

